Lab on a Chip

Devices and applications at the micro- and nanoscale

Accepted Manuscript

This article can be cited before page numbers have been issued, to do this please use: S. Hu, B. Zhang, S. Zeng, L. Liu, K. Yong, H. Ma and Y. Tang, *Lab Chip*, 2020, DOI: 10.1039/D0LC00202J.

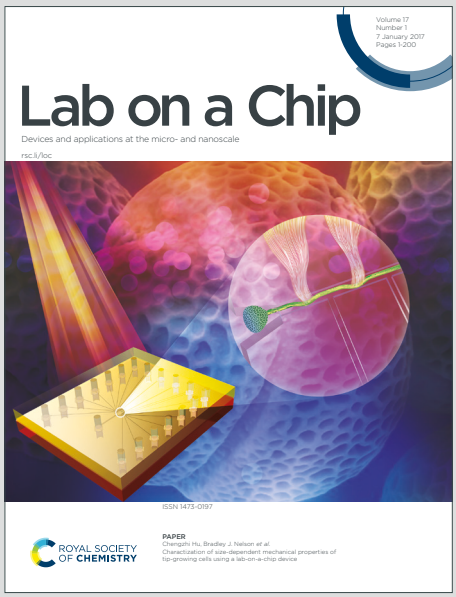

ROYAL SOCIETY OF CHEMISTRY

rsc.li/loc

View Article Online
DOI: 10.1039/D0LC00202J

ARTICLE

Microfluidic Chips Enabled One-step Synthetization of Biofunctionalized $CuInS_2$/ZnS Quantum Dots

Received 00th January 20xx,
Accepted 00th January 20xx

DOI: 10.1039/x0xx00000x

Siyi Hu,[a] Butian Zhang, [d] Shuwen Zeng, [e] Liwei Liu, [c] Ken-Tye Yong,*[b] Hanbin Ma,*[a] Yuguo Tang [a]

Biofunctionalized quantum dots (QDs) are effective targeted fluorescent labels for bioimaging. However, conventional synthesis of biofunctionalized I-III-VI core-shell $CuInS_2$/ZnS QDs requires complex bench-top operations, results in limited product performance and variety, and is not amenable to a 'one-step' approach. In this work, we have successfully demonstrated a fully automated method for preparing denatured bovine serum albumin (dBSA)-$CuInS_2$/ZnS QDs by introducing microfluidic chips (MF) to synthesize biofunctionalized QDs, hence establishing a 'one-step' procedure. We have also studied and optimized the reaction synthesis parameters. The emission wavelength of dBSA-$CuInS_2$/ZnS QDs is located in the near-infrared range and can be tuned from 650 to 750 nm by simply varying the reaction parameters. In addition, the 'one-step'-synthesized dBSA-$CuInS_2$/ZnS QDs have a long average fluorescence lifetime of 153.76 ns at a small particle size of 5±2 nm. To demonstrate the applicability of the 'one-step'-synthesized dBSA-$CuInS_2$/ZnS QDs in bioimaging studies, we modified the QDs with folic acid and hyaluronic acid, and then performed target bioimaging and cytotoxicity tests on macrophages, liver cancer cells and pancreatic cancer cells. The cell images show that the red emission signals originate from the QDs, which indicates that the dBSA-$CuInS_2$/ZnS QDs prepared by the MF approach are suitable optical contrast agents for target bioimaging. This 'one-step' MF-based QD synthesis approach could serve as a rapid, cost-effective, and small-scale nanocrystal production platform for complex QD formulations for a wide range of bioapplications.

Introduction

Quantum Dots (QDs) have achieved widespread use in biomedical applications owing to the rapid development of their synthesis and biofunctionalization methods. In the past decade, cadmium-free I-III-VI QDs have been used in bio-application studies due to their low biotoxicity and environmentally friendly natures[1]. I-III-VI QDs, such as $CuInS_2$ and $AgInS_2$, which are cadmium-free QDs. In particular, $CuInS_2$ QDs not only have low biotoxicity but also possess additional chemical and physical properties such as a long photoluminescence (PL) lifetime, a large Stokes shift, a high extinction coefficient, and adjustable PL potential in the visible-near-infrared region[1-3].

According to related reports, $CuInS_2$ QDs are usually prepared in the oil phase, and studies of the aqueous phase method are relatively rare. The main barriers to the synthesis of aqueous-phase $CuInS_2$ QDs are as follows:1) The reaction temperature needs to be very precise; 2) The reaction time needs to be more than 4 hours; 3) Cuprous ions are easily oxidized and need to be handled carefully during the reaction[4]. However, with the development of technology, some of the problems encountered in the synthesis of QDs can be solved by a new method, such as microfluidics technology.

Microfluidics (MF) has become a powerful tool for QD synthesis and has several advantages over the bench-top(BT) method[5], such as minimal use of chemicals, reduced the raw materials, decreased reaction time, the possibility of carrying out several reactions at once, precisely controlled reaction conditions, rapid heat transfer due to the large surface-to-volume ratios of the MF channels, and high integration[6, 7]. The first nanoparticle synthesis by MF chips was reported by Prof. Andrew deMello's group in 2002[8]; they applied continuous flow-based MF chips to successfully synthesize CD's nanoparticles. Since then, many kinds of metallic[9, 10], metal oxide [11], magnetic[12] and Quantum dots nanoparticles [13-17] have been successfully prepared by MF chips.

Among the abovementioned materials, colloidal QDs have attracted much attention from researchers in the field of MF due to their unique physicochemical properties, and these QDs have many applications in the biomedical field[18]. For the bio-application of QDs, researchers have always modified the QDs with biofunctional molecules to make them biocompatible[19];

[a] CAS Key Laboratory of Bio-medical Diagnostics, Suzhou Institute of Biomedical Engineering and Technology, Chinese Academy of Sciences, No.88 Keling Road, Suzhou, Jiangsu, 215163, P.R. China.
[b] School of Electrical and Electronic Engineering, Nanyang Technological University, Singapore 639798, Singapore.
[c] Key Laboratory of Optoelectronic Devices and Systems of Guangdong Province, College of Optoelectronic Engineering, Shenzhen University, Shenzhen 518060, China.
[d] MOE Key Laboratory of Fundamental Physical Quantities Measurement, PGMF and School of Physics, Huazhong University of Science and Technology, Wuhan 430074, P. R. China.
[e] XLIM Research Institute, UMR 7252 CNRS/University of Limoges, Limoges, 87060, France
* Corresponding author: mahb@sibet.ac.cn ; ktyong@ntu.edu.sg .
Electronic Supplementary Information (ESI) available: [details of any supplementary information available should be included here]. See DOI: 10.1039/x0xx00000x

the whole process in the conventional BT method is very complicated[20]. However, very little success has been realized by applying the BT method to synthesize biofunctionalized QDs in a single step[21]. Thus, MF chips with the advantage of high integrability can be modified with different functional units to simultaneously synthesize and biofunctionalized nanomaterials in a one-step experiment[22].

In this work, we report the use of a MF chip for the one-step synthesis of biofunctionalized core/shell heavy metal-free denatured bovine serum albumin (dBSA)-$CuInS_2$/ZnS QDs. We have studied and optimized the reaction synthesis parameters. The emission wavelength of dBSA-$CuInS_2$/ZnS QDs is located in the near-infrared range and can be tuned from 650 to 750 nm by simply varying the reaction parameters. The prepared QDs were then characterized by TEM, lifetime decay, and agarose gel electrophoresis. Because of the excellent liquid handling capabilities of the MF approach, the prepared QDs exhibit a high photostability and colloidal stability. To demonstrate the applicability of the 'one-step'-synthesized dBSA-$CuInS_2$/ZnS QDs in bioimaging studies, we modified the QDs with folic acid (FA) and hyaluronic acid (HA) and then performed target bioimaging and cytotoxicity tests on macrophages, liver cancer cells and pancreatic cancer cells.

Results and discussion

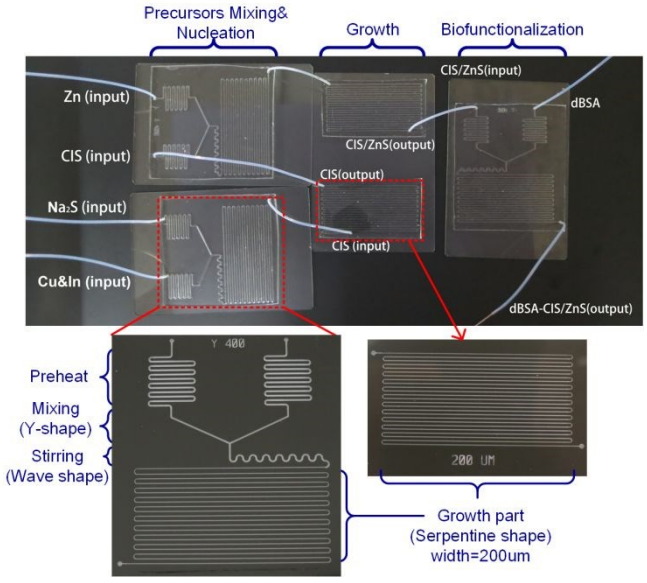

Figure 1. The physical and mask picture of the fabricated MF platform

In our one-step synthesis of biofunctional QDs by using microfluidic chips. The microfluidics chips we designed and fabricated a polydimethylsiloxane (PDMS)/glass MF chip containing three kinds of microflow structure, which are Y-shape, wave shape and serpentine shape microchannel. We applied serpentine shape to preheat the reaction precursor solution and to react the growth of QDs after nucleation. The Y-shape microchannels are used for mixing of precursor solution and nucleation of QDs. And the wave shape microchannel is mainly used to rapidly flow the solution of QDs after nucleation, through this channel to achieve the stirring function, so that the QDs after nucleation can be dispersed in the reaction system to achieve well dispersion of the final product.

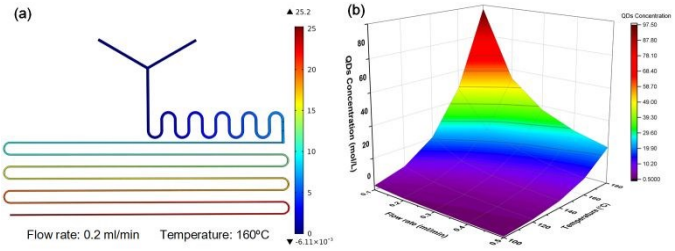

Figure 2. (a) the simulation model and the simulation result of the reaction temperature of 160°C and the flow rate of 0.2 ml/min, (b)The simulation study of the concentration distribution of the QDs synthesized by the microfluidic chips with different reaction temperature (100°C, 120°C, 140°C, 160°C and 180°C) and flow rate (0.1, 0.2, 0.3, 0.4 and 0.5 ml/min).

In this work, we first did the simulation study to investigate the influence of the flow rate and reaction temperature on the growth rate of QDs in the microfluidics chips. By using the Reaction Engineering (*re*), Chemistry(*chem*), transport of diluted species (*tds*), and laminar flow (*spf*) models in Comsol Multiphysics 5.4, the relationship between the yield of QDs and reaction condition (i.e. the flow rate and reaction temperature in the microfluidics chip) can be theoretically predicted. The geometric reduced model and the distribution profiles of the concentration of QDs synthesized in this Y-shape microfluidic chips, as shown in figure 2(a). And we have collected the value of the QDs concentration with different reaction temperature and flow rate at the end of the microfluidic channel, then the data have been plotted in figure 2(b). From the figure 2(b), we can see, the QDs concentration increased with the increasing of reaction temperature and the decreasing of flow rate. According to the simulation study, we know that when the reaction temperature is 160 degrees, and the flow rate is 0.2mL/min, more quantum dots can be obtained. Although more quantum dots can be obtained at 180 degrees, the PDMS chip is prone to damage at 180 degrees. We then carried out the QDs synthesis experiment with microfluidic chips under the same reaction temperature and flow rate to proof the simulation results.

View Article Online
DOI: 10.1039/D0LC00202J

ARTICLE

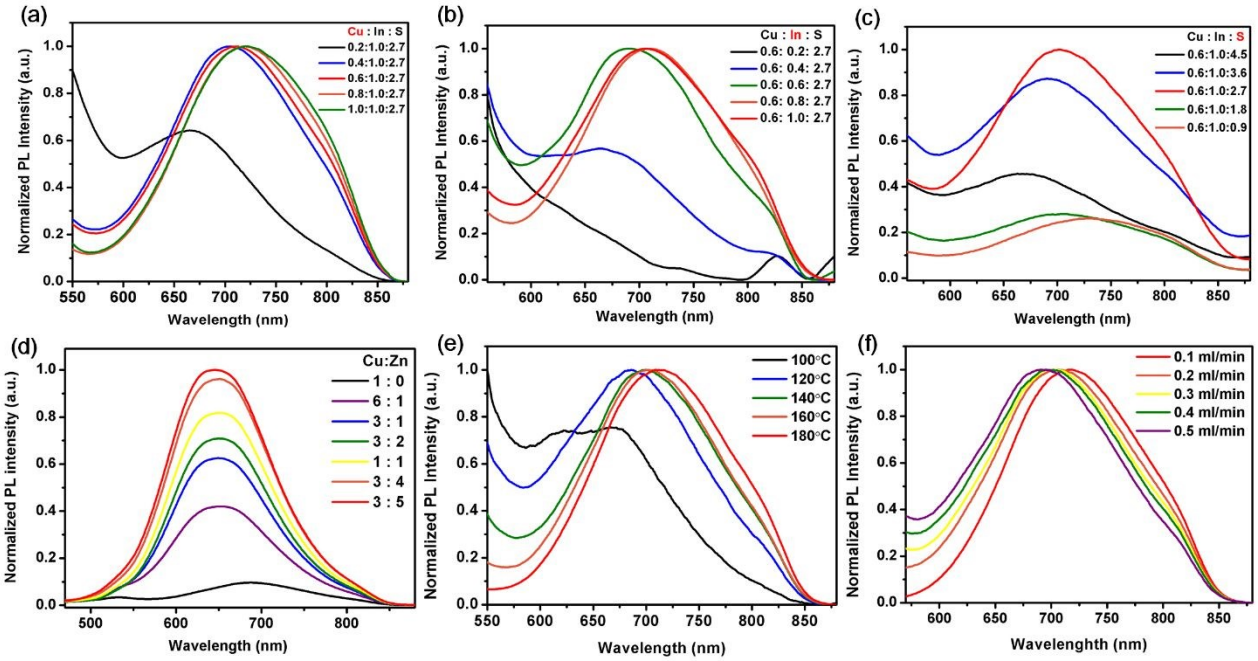

Figure 3. The photoluminescent (PL) spectrum of the optimized the reaction parameters of synthesis the $CuInS_2$ and $CuInS_2$/ZnS QDs in Y-shape microfluidic chips. Changing the (a)Cu (b) In (c) S (d) Zn mole fraction ratio, (e) the reaction temperature and flow rate of synthesis $CuInS_2$ and $CuInS_2$/ZnS QDs

In our one-step synthesis of $CuInS_2$/ZnS (CIS/ZnS) QDs using the MF chip approach, 3-mercaptopropionic acid (MPA) was used as the surface ligand to stabilize and control the growth of QDs in the aqueous phase. In contrast to the traditional BT water-phase synthetic method, this method is more efficient and simpler, and the reaction conditions can be more precisely controlled. Because the reaction conditions are different from those of the traditional synthesis method, the previous reaction parameters are not very suitable for the MF chip method. Therefore, in this work, we first investigated the effects of various Cu:In:S molar ratios in the MF chip method because the Cu:In ratio is the major factor contributing to bulk defects or creating internal defects during the synthesis of $CuInS_2$ (CIS) QDs. Based on the PL spectra in figure 3 (a) (b) and (c), we chose a Cu:In:S molar ratio of 0.6:1:2.7. Based on a previous study, we know that the CIS QDs can be coated with ZnS shells, resulting in an enhancement of the fluorescence intensity and a blueshift of the CIS peak in the PL spectrum. We also applied MF chips to synthesize core-shell CIS/ZnS QDs in one step, and we varied the Cu:Zn ratio; from figure 3(d), we can see that as the proportion of Zn increased, the PL intensity increased, and the PL peaks blue shifted, consistent with the results of the bench-top method. However, the whole process utilizing MF chips requires only 5 minutes, which is less than the time required for the bench-top methods (>1 hour).

After we optimized the element ratio for the one-step synthesis of CIS/ZnS QDs in the MF chips, we optimized the reaction temperature and the flow rate for this approach, as shown in figure 3(e) and (f). With increasing temperature and decreasing flow rate, the PL peaks of the QDs were redshifted. This result indicated that a high temperature could increase the reaction efficiency and that a low flow rate could increase the reaction time, leading to the complete reaction of the QDs. However, the reaction parameters also have threshold values. After repeated testing, we chose a reaction temperature of 160 °C and a flow rate of 0.2 mL/min for the synthesis of CIS/ZnS QDs.

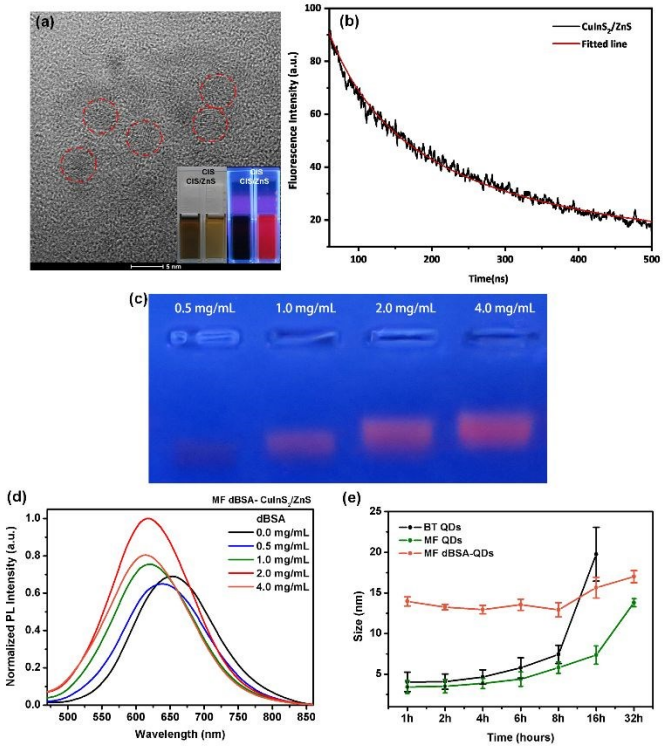

Figure 4. (a) TEM image of $CuInS_2$/ZnS QDs and digital images of $CuInS_2$ and $CuInS_2$/ZnS QDs obtained without and with UV irradiation. (b) Lifetime decay curves of $CuInS_2$/ZnS QDs and the fitting line. Agarose gel electrophoresis image(c) and PL spectrum (d) of dBSA-$CuInS_2$/ZnS QDs synthesis by microfluidics chips with different concentration of dBSA. (e)Comparison of photostability of $CuInS_2$/ZnS (QDs) and dBSA-$CuInS_2$/ZnS (dBSA-QDs) prepared by the BT method and the MF method

Figure 4(a) shows the TEM image of $CuInS_2$/ZnS QDs and digital images of $CuInS_2$ and $CuInS_2$/ZnS QDs. From the image, we can also see that after coating the $CuInS_2$/ZnS QDs with a ZnS shell, the fluorescence intensity of the coated QDs is stronger than that of $CuInS_2$. From the TEM figure, we can see that the $CuInS_2$/ZnS QDs have an average size of approximately 5±2 nm, a relatively uniform size distribution and a clear lattice structure, the HRTEM picture of the CIS/ZnS QDs as shown in figure S1(a). The alloyed structure of the microfluidic synthesized $CuInS_2$ and CIS/ZnS QDs was investigated by the XRD spectroscopy, as shown in figure S1(b). The XRD peaks of the CIS QDs have the typical diffraction peaks of the tetragonal $CuInS_2$ pattern (JCPDS 27-0159). After coated with the ZnS shell, the diffraction peaks of the CIS/ZnS QDs shifted to the larger angels and have the typical diffraction peaks of the ZnS (JCPDS 05-0566), the XRD results show that the application of microfluidic chips can achieve effective coating of ZnS shell. To further prove that the CIS/ZnS QDs synthesized by the MF chip have good optical properties, we also measured their fluorescence lifetime spectrum. Figure 4(b) shows the fluorescence lifetime decay and fitting curve for CIS/ZnS QDs. The fitting curve is obtained by the following quadratic exponential fitting formula.

$$\boldsymbol{F(t) = B_1 exp\,(-t/\tau_1) + B_2 exp\,(-t/\tau_2)} \quad (1)$$

The average fluorescence lifetime is calculated by formula (2):

$$\boldsymbol{\tau = (B_1\tau_1^2 + B_2\tau_2^2)/(B_1\tau_1 + B_2\tau_2)} \quad (2)$$

B_1 and B_2 represent the weights of the fluorescence lifetimes of each group, where B_1=5.846% and B_2=94.154%; τ_1 and τ_2 represent time constants, where τ_1=5.96 ns and τ_2=154.13 ns. The generation of τ_1 originates from the nonradiative recombination of the surface defects of the QDs and the radiation of the electron-hole pairs, which is the fast portion of the fluorescence lifetime. The generation of τ_2 is derived from the process in which the doublet decays to the ground state, which is the slow portion of the fluorescence lifetime and is also the part that contributes to the fluorescence lifetime of the QDs, resulting in a longer fluorescence lifetime for the QDs. The average fluorescence lifetime of CIS/ZnS QDs calculated by formula (2) is 153.76 ns.

The main application of near-infrared CIS/ZnS QDs is bioimaging. Therefore, in addition to having good near-infrared optical properties, these QDs also need to have good biocompatibility, such as low toxicity, easy biomodification and high photostability. In our previous paper, we demonstrated that BSA could be used as a stabilizer to synthesize BSA-CdTe QDs in MF chips[13]. From the experimental process, we found that dBSA could increase the PL intensity of QDs. Because dBSA is a kind of biomacromolecule that contains 35 cysteine residues, which can be used as stabilizer to interact polyvalent with QDs, we can prepare chemically reduced BSA[23, 24]. The dBSA also makes the QD surface more biofunctional and simultaneously reduces the toxicity of the QDs[25, 26]. Therefore, we applied MF chips (as shown in figure 1) to successfully synthesize dBSA- CIS/ZnS QDs in one step. In the synthesis process, we varied the concentration of dBSA in the reaction.

To further investigate the binding efficiency of different concentrations of dBSA and QDs, gel electrophoresis was used, as shown in figure 4(c). As the concentration of dBSA increased, the distance between the initial hole and the band of dBSA-QDs gradually decreased, which means that the molecular weight of the finally obtained dBSA-QDs gradually increased. Figure 4(d) shows the PL intensity of the dBSA-QDs synthesized with different concentrations of dBSA. The PL intensity increased with increasing dBSA concentration, but when the dBSA concentration was 4 mg/mL, the PL intensity decreased, which may be because the stabilizers around the QDs were saturated. If the excessive stabilizer was present, the PL intensity of the QDs was decreased. Therefore, in subsequent experiments, we applied dBSA of 2mg/mL.

The photostability of QDs is an important factor to be considered when utilizing them as optical probes for bioimaging. Figure 4(e) shows the hydrodynamic sizes of CIS/ZnS QDs produced by the BT and MF methods and the dBSA-$CuInS_2$/ZnS QDs produced by the MF method. These samples were exposed to continuous UV light radiation for 32 hours. The hydrodynamic sizes were monitored by dynamic light scattering

(DLS) at room temperature. More specifically, after 16 hours of UV radiation, the particle size increased by 70% for the QDs generated by the MF method, but an increase of 400% was observed for the QDs generated by the BT method. At the same time, we also monitored the change of PL spectrum for 10 hours, and the results showed that the PL intensity of MF QDs decreased less than that of BT QDs, the results as shown in figure S5. This clearly shows that the photostability of QDs prepared using the MF method is significantly better than that of QDs prepared by the BT method. This is because MF method can accurately control reaction temperature and time at first; The secondly, it has a high surface-to-volume ratio, which increase the reaction efficiency and makes the reaction of coating ZnS shell and dBSA modification complete; Finally, the nucleation process can be precisely controlled to make the precursor solution fully and rapidly mixing, which improves the nucleation efficiency[27]. The above advantages effectively improve the quality of the obtained QDs and thereby improve the photostability of QDs.

As shown in figure 4(e), another set of comparative experiments were performed to compare the photostability of CIS/ZnS QDs and dBSA-CIS/ZnS QDs synthesized by the MF method. After monitoring for 32 hours, the particle size increased by 15% for the dBSA-QDs and by 200% for the QDs. Therefore, the photostability of the dBSA-QDs prepared by the MF method is significantly higher than that of the QDs fabricated by the same method because dBSA is rich in cysteine groups and can act as a stabilizer for QDs, thus preventing the agglomeration or precipitation of QDs by balancing the activity of cuprous and indium ions in the QDs. The surface of the QDs can be modified by coordination between the sulfhydryl groups of the surface cysteine groups and the metal ion to enhance the water solubility of the QDs, promote their dispersion in water, and avoid precipitation. Moreover, through a comparative analysis of the quantum dot yield, it can also be found that the quantum dots synthesized by the microfluidic chip is also significantly higher than the BT method, and dBSA also effectively improves the quantum yield, as shown in table S1.

As mentioned above, we have demonstrated the QDs prepared by MF have better optical stability and colloid stability, and the emission wavelength is in the near infrared region, which make them can be the candidate PL probe in the in vitro bioimaging study and biosensor detection application. In order to prove that the dBSA-CIS/ZnS QDs synthesized by MF method are convenient for specific biological functionalization and can be used for in vitro target cell imaging study in near infrared wavelength. Here, we selected macrophage cells (RAW264.7), pancreatic cancer cells (Panc-1) and liver cancer cells (HepG-2) for in vitro bioimaging studies. According to the previous study, specific cell imaging of Panc-1 can be achieved by modifying the surface of QDs with folic acid(FA)[13]. And for the HepG-2 cell, there are some researchers have found that Hyaluronic Acid (HA) has a good specificity[28]. Therefore, in this study, FA and HA, two commonly used cancer cell targeting molecules, were selected to perform surface-specific biofunctionalization on the dBSA-CIS/ZnS QDs, and the modified QDs were applied to in vitro cell imaging and cytotoxicity studies.

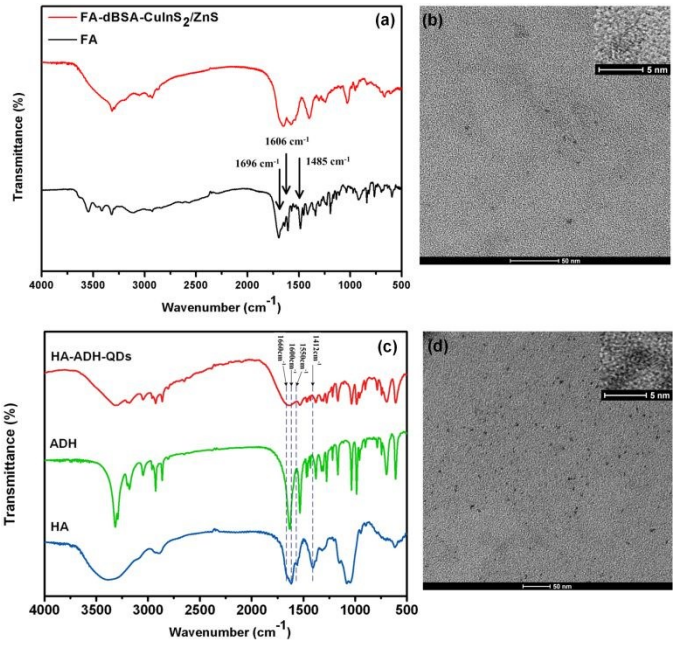

Figure 5. The FT-IR spectra and TEM images of FA-modified dBSA- $CuInS_2$/ZnS QDs (a, b) and HA-modified dBSA-$CuInS_2$/ZnS QDs (c, d)

To confirm the combination of HA and FA biomolecules with the dBSA-CIS/ZnS QDs, Fourier transform infrared (FT-IR) spectra and TEM images were used to characterize the QDs. Figure 5(a) shows the FT-IR spectra of FA-dBSA-CIS/ZnS QDs and FA powder. From the spectra, we can see that FA has vibration peaks at 1696 cm^{-1} (C=O bond), 1606 cm^{-1} (-NH group), and 1485 cm^{-1} (benzene ring). The intensity of these three peaks is weaker and the peaks become broader for FA-dBSA-QDs than for FA, which indicates that a combination of covalent bonds occurs at the above three positions. These results prove that FA is effectively combined with dBSA-QDs mainly through covalent bonds.

For the HA combination, as shown in figure 5(c), HA has obvious vibration peaks or characteristic peaks at 1660 cm^{-1}, 1600 cm^{-1}, 1550 cm^{-1}, and 1412 cm^{-1}, of which the peaks at 1600 cm^{-1} and 1412 cm^{-1} are assigned to the asymmetric and symmetric vibrational peaks of the carboxyl group, and those at 1600 cm^{-1} and 1550 cm^{-1} are characteristic peaks of the amide I and amide II bonds, respectively. In the FT-IR spectrum of HA-ADH-QDs, compared with that of HA, the peaks broaden, and the characteristic peaks disappear, indicating that the QDs combined with HA through the carboxyl groups and amides via covalent bonds.

We also performed TEM characterization of the samples. Figures 5(b) and 5(d) show the TEM images of QDs modified by FA and HA, respectively. The modified QDs still have a good lattice and morphological structure, and the QDs themselves remain approximately 5 nm in size. The particle size and surface lattice structure did not show significant changes, no obvious

agglomeration occurred after modification, and the dispersion was uniform. The hydrodynamic size distribution of MF CIS QDs, MF CIS/ZnS QDs, FA-QDs and HA-QDs in aqueous suspension measured by dynamic light scattering (DLS), the results as shown in figure S2, which indicated the prepared QDs have good dispersion, and the zeta potential of the prepared QDs have been shown in figure S3. The zeta potential of FA and HA modified QDs were all negatively charged, and the zeta potential were close to -30mV, indicating that they have good stability and suitable for the bioimaging study. We also applied PL spectrum to characterize FA-QDs and HA-QDs, the PL spectrum of HA-QDs and FA-QDs are blue-shifted compared to the spectra of dBSA-QDs, which proved that HA or FA were successfully modified on the surface of dBSA-QDs, and still had good photoluminescent properties, the PL spectrum as shown in figure S4.

For the bioimaging study, a preliminary assessment of the use of dBSA-CIS/ZnS, FA-dBSA-CIS/ZnS and HA-dBSA-CIS/ZnS QDs for bioimaging was first performed using RAW264.7 macrophages. Because macrophages are sensitive to the surrounding environment and have no specificity for PL probes, they can be used to evaluate the biological compatibility and toxicity of PL probes. As illustrated in figure 6(a), the control group did not interfere with near-infrared autofluorescence under the excitation of the blue light without adding any sample. Strong cellular uptake was observed for the dBSA-QD, FA-dBSA-QD and HA-dBSA-QD formulations, and the concentration of QDs is 25μg/mL. The red emission signals originated from the QDs. At the same time, the cell state of the experimental group remained good compared with the cell state of the control group, and there was no change in cell morphology or cell wall damage, indicating that the cytotoxicity of these three kinds of QDs is relatively low. To further demonstrate the cellular activity of these three kinds of QDs on macrophages, the cytotoxicity was further tested by the MTT assay. The results are shown in figure 6(b). The cadmium-free QDs exhibited a significantly lower toxicity than the cadmium-containing dBSA-CdTe QDs. At concentrations less than 100 μg/mL, the toxicity of dBSA-QDs, FA-dBSA-QDs and HA-dBSA-QDs were all greater than 70%, which indicates that these three kinds of QDs are suitable for cell imaging studies.

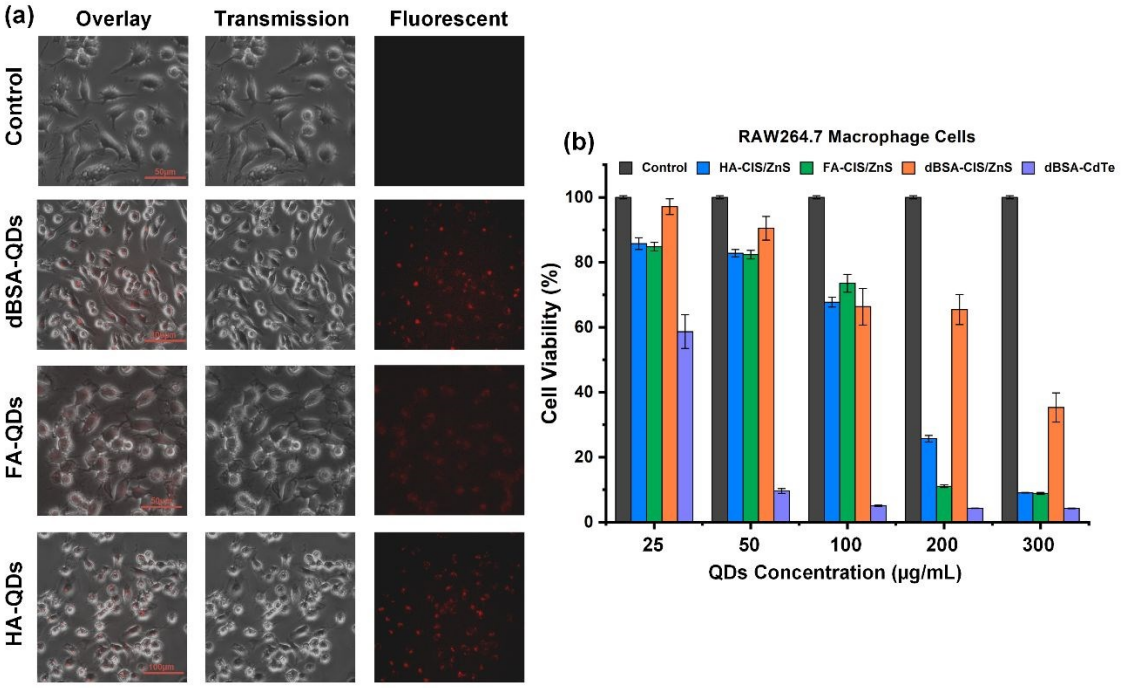

Figure 6. Microscope images (a) and cell viability (b) of RAW264.7 cells

According to the cell imaging and toxicity study results of macrophages, the HA-dBSA-QDs and FA-dBSA-QDs were applied for the further specific target imaging of cancer cells. Cell imaging of HepG-2 cells with HA-dBSA-QDs was performed, and the images are shown in figure 7(a); the first line is the control group, and there is no autofluorescence interference in the near-infrared emission range. The second line shows the QDs without HA modification, and there is no obvious red fluorescence signal in the cells, indicating that the QDs without HA modification did not enter the cells for labelling. In the HA-QD experiment group, there is a clear red fluorescence signal in the cells. Compared with that of the control group, the cell morphology in the group treated with HA-QDs remained basically the same, indicating that the HA-QDs have a specific labelling effect on HepG-2 cells. From the toxicity experiment results, shown in figure 7(b), we can also see that HA-QDs have low cytotoxicity to HepG-2 cells and can be used as specific fluorescent biomarkers for targeted bioimaging studies of liver cancer cells.

View Article Online
DOI: 10.1039/D0LC00202J

ARTICLE

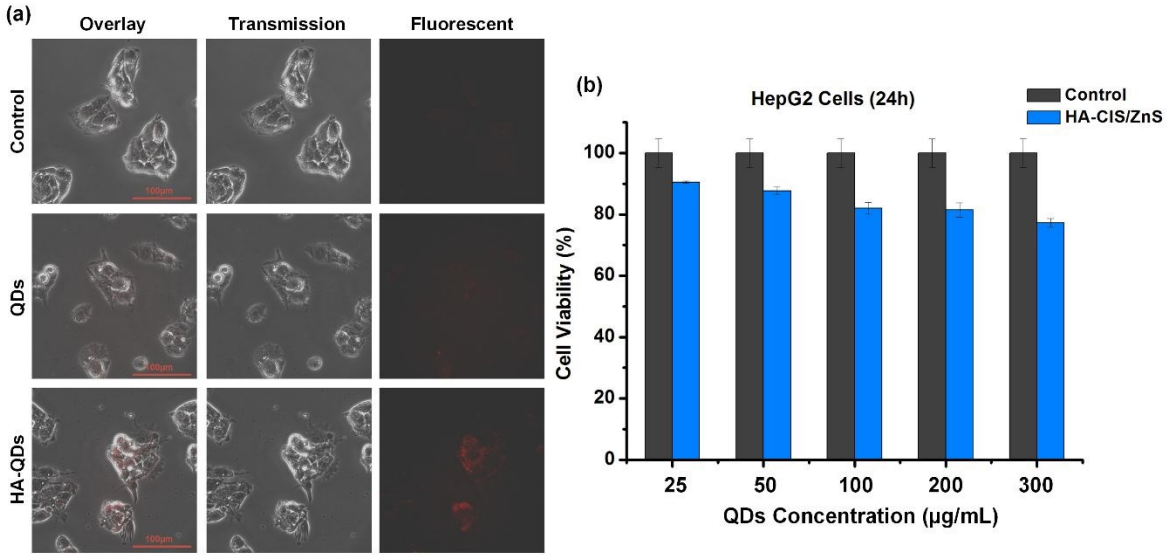

Figure 7. Microscope images (a) and cell viability (b) of HepG-2 cells

Then, cell imaging of Panc-1 pancreatic cancer cells with FA-dBSA-QDs was performed. The experimental method was similar to that used for the HepG-2 cells. Fluorescence imaging of Panc-1 cells, as shown in figure 8(a), was obtained under blue light excitation at a wavelength of 450 nm. In the control group, the cells showed no autofluorescence interference in the near-infrared emission range, and the second line shows the QDs without FA modification. After addition of the QDs to the Panc-1 cells, no fluorescent signal was observed, indicating that the QDs are not specific to the Panc-1 cells. The FA-QDs show a clear red fluorescence signal in the dark-field fluorescence image of Panc-1 cells. Moreover, the cell state remained good compared to that of the control group, indicating that the toxicity of this material has no effect on cell health, as demonstrated by the cytotoxicity test in figure 8(b).

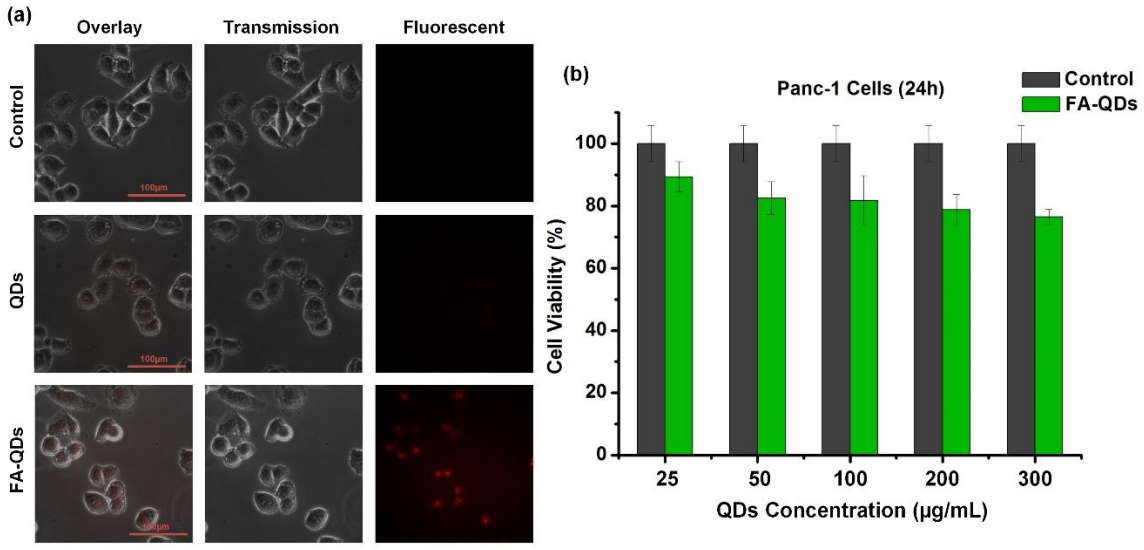

Figure 8. Microscope images (a) and cell viability (b) of Panc-1 cells

Experimental

Materials

Copper(II) chloride ($CuCl_2$, 99%), indium(III) chloride tetrahydrate ($InCl_3 \cdot 4H_2O$, 97%), zinc acetate ($Zn(Ac)_2$, 99.99%), 3MPA (≥99%), ammonium hydroxide solution (NH_4OH, 28.0%-30.0%), BSA (≥98%), FA (≥97%), N-hydroxysuccinimide (NHs, 98%), 1-(3-dimethylaminopropyl)-3-ethylcarbodiimide hydrochloride (EDC), adipic dihydrazide (ADH) and dimethyl sulfoxide (DMSO) were purchased from Sigma-Aldrich. Sodium sulfide hydrate ($Na_2S \cdot xH_2O$, 60-63%) was obtained from ACROS Organics. Sodium hydroxide (NaOH, AR) and hydrochloric acid (HCl, AR) were purchased from Sinopharm Chemical Reagent Co., Ltd. 10× Tris-acetate-EDTA (TAE, pH=8.0) and agarose powder were purchased from Vivantis Ltd. Sodium hyaluronate (HA) with a mass of 215 kDa was purchased from American Lifecore Company. All chemicals were used as received without further purification. The deionized (DI, 18.2 MΩ•cm) water used in all the studies was purified by a Milli-Q water purification system.

Design and fabrication of MF chips

The MF chips were fabricated through soft lithography and replica molding methods based on previous research [13]. Briefly, the negative photoresist SU-8 (GM1070, Gersteltec Engineering Solutions, Switzerland) was spin coated onto a 4-inch silicon wafer, followed by UV patterning of the channels (3 minutes, lamp power: 355 W). The patterned wafer was developed using an AZ developer (Branchburg, NJ) to remove the unexposed photoresist to form an SU-8 model. A PDMS mixture containing curing agent and base resin (Dow Corning, US) with a weight ratio of 1:10 was poured onto the model and cured at 120 °C for 10 minutes. The cured PDMS layer with MF channels was then carefully peeled off, and finally, the PDMS layer was bonded to a glass slide by means of a plasma process.

MF synthesis of aqueous-phase $CuInS_2$, $CuInS_2$/ZnS and dBSA-$CuInS_2$/ZnS

First, Cu^+ and In^{3+} mixed solutions were prepared. The Cu^+ precursor was prepared by dissolving 18 mg of $CuCl_2$ in 0.5 mL of ammonia water and 180 µL of MPA mixed solution to obtain a clear Cu^+ solution. The In^{3+} precursor was prepared by dissolving $InCl_3 \cdot 4H_2O$ in 10 mL of DI water containing 68 µL of MPA and then adjusting the pH of the In^{3+} solution to 10 with NaOH. Then, the Cu^+ precursor and In^{3+} precursor were mixed and stirred for 5 minutes and transferred to a 10 mL syringe. Second, the Na_2S solution was prepared by dissolved 72 mg of Na_2S in 10 mL of DI water and then placed in a 10 mL syringe. Third, the Zn^{2+} precursor was prepared by dissolving 7 mg of $Zn(Ac)_2$ in 10 mL of DI water containing 5 µL of MPA, adjusting the pH to 10 with NaOH, and then loading the solution into a 10 mL syringe. Fourth, a 30 mL dBSA solution was prepared with a concentration of 16 mg/mL by a reaction between BSA at 70° and $NaBH_4$ to obtain dBSA. Finally, the MF chip was placed on a hot plate, and the dBSA modifier was placed on another hot plate, and the temperatures were adjusted to 160 °C and 80 °C, respectively. After preheating for 5 minutes, the above Cu^+ and In^{3+} mixed solution and the syringes of Na_2S and Zn^{2+} precursors were placed into the multichannel microinjection. On the pump, the propulsion speed was set to 0.2 mL/min, and the syringes were connected to the corresponding channel inlet to start the syringe pump. The syringe containing dBSA was placed on another single-channel syringe pump, and the advancement speed was adjusted to 0.5 mL/min. When the $CuInS_2$/ZnS QDs exit at the $CuInS_2$/ZnS outlet, the dBSA syringe pump was started. A sample vial was placed at the end of the system to collect the final dBSA-$CuInS_2$/ZnS product. The collected dBSA-$CuInS_2$/ZnS QDs were purified by 50 kDa cut-off ultrafiltration tubes and centrifuged at 8000 rad/min for 10 minutes.

Biomodification of dBSA-$CuInS_2$/ZnS QDs by FA and HA.

The biomodification methods were previously reported[29, 30]. Briefly, for FA modification, 4 mL each of a 2.3 mg/mL EDC solution and a 3.86 mg/mL NHs solution were prepared, and 6 mg of FA was dissolved in 3 mL of DMSO solution to obtain a 2 mg/mL FA solution. Then, 100 µL of EDC was added to a 2 mg/mL QD solution and stirred for 2 minutes, and then 100µL of NHs was added and stirred for 2 minutes to activate the amino group on the surface of the QDs. Finally, 600 µL of 2 mg/mL FA solution was added to the activated QD solution and stirred for 3 hours. The FA-dBSA-$CuInS_2$/ZnS QDs were purified by centrifugation at 8000 rad/min for 10 minutes using a 3 kDa cut-off ultrafiltration tube.

For HA modification, a HA-ADH solution must first be prepared[31, 32]. First, 50 mg of HA was dissolved in 10 mL of DI water, 0.92 g of ADH was added to the HA solution, the pH of the HA-AD solution was adjusted to 4.8 with HCl, and the solution was stirred for 30 minutes. Next, 0.1 g of EDC powder was added, the solution was stirred for 2 hours, the pH was adjusted to 7 by adding NaOH, and the reaction was stopped. The solution was dialyzed in a 3 kDa dialysis bag for 24 hours, and the precipitate was washed with ethanol to obtain pure HA-ADH for use. Second, 4 mL each of a 2.3 mg/mL EDC solution and a 3.86 mg/mL of NHs solution were prepared, and 7 mg of HA-ADH was dissolved in 3 mL of DI water to obtain a 2.3 mg/mL HA-ADH solution. Third, 100 µL of EDC and 100 µL of NHs were added in sequence to 2 mL of dBSA-$CuInS_2$/ZnS QD solution and stirred for 2 minutes. Then, 3 mL of 2.3 mg/mL HA-ADH was added to the activated QD solution and stirred for 4 hours. The prepared HA dBSA-$CuInS_2$/ZnS QDs were centrifuged and purified by a 50 kDa cut-off ultrafiltration tube at 8000 rad/min for 10 minutes.

Cell Imaging study

RAW264.7 macrophages, Panc-1 pancreatic cancer cells and HepG-2 liver cancer cells were obtained from the American Type Culture Collection (ATCC). The materials used in the cell experiments were DMEM high-sugar medium, RPMI-1640 medium, and fetal bovine serum (FBS) purchased from HyClone and penicillin and streptomycin purchased from Gibco. The cells were cultured as follows:

1) RAW264.7 macrophages and Panc-1 pancreatic cancer cells

Cell culture was carried out using DMEM high-glucose medium containing 10% FBS, 100 µg/mL penicillin, and 100 µg/mL streptomycin. The cells were used after a cell density of 70% was achieved in a 5% CO_2, saturated humidity, 37 °C cell culture incubator.

2) HepG-2 liver cancer cells

Cell culture was carried out using RPMI-1640 medium containing 10% BSA, 100 μg/mL penicillin, and 100 μg/mL streptomycin. The cells were used after a cell density of 70% was achieved in a 5% CO_2, saturated humidity, 37 °C cell culture incubator.

3) Cell imaging

Cells were first digested with 0.25% trypsin and then seeded in 6-well plates. The cells before the experiment need to be cultured for 24 hours, and the density was approximately 60% to 70%. The QD samples used for imaging were dissolved in PBS at a concentration of 100 μg/mL (pH = 7.2). Then, 20~40 μL of sample was added to each well of the 6-well plates, shaken gently, and incubated for 4 hours at 37 °C in 5% CO_2. The culture solution was then removed, and the samples were washed with PBS 3 times. An inverted fluorescence microscope was used to observe the cell morphology and perform fluorescence imaging

Cell viability study

(3-(4,5-Dimethylthiazol-2-yl)-2,5-diphenyltetrazolium bromide salt (MTT), purchased from Sigma Company, was used for colorimetric analysis. After dissolving dBSA-CdTe, dBSA-$CuInS_2$/ZnS, FA-dBSA-$CuInS_2$/ZnS and HA-dBSA-$CuInS_2$/ZnS QDs at concentrations of 25, 50, 100, 200, and 300 μg/mL in PBS, 4 μL of each mixture was added to a well plate, shaken and cultured at 37 °C in 5% CO_2 for 24 hours. After 24 hours, 18 μL of 5 mg/mL MTT solution was added to each well, shaken, and cultured at 37 °C in 5% CO_2 for 4 hours. After aspirating the solution in each well, 150 μL of DMSO was added. The plate was scanned at 490 nm using a Bio-Rad plate reader. The final cell viability data were obtained by normalizing the absorbance values of each well and comparing them with the reference control sample wells.

Conclusions

In summary, we presented a detailed study on applying an MF chip for the synthesis of $CuInS_2$, $CuInS_2$/ZnS, and dBSA-$CuInS_2$/ZnS QDs. The microfluidics chips were fabricated by soft lithography and replica molding methods, which include the Y-shape, wave-shape and snake shape structure in the chips, the minimum microflow channel width is 200um. The MF method is quite different from the traditional method in terms of chemical reaction conditions. Therefore, the MF chip synthesis should be optimized based on the Cu:In:S ratio and the reaction condition in the passivation reaction. After optimization, we found that the reaction concentration for the MF method is the Cu:In:S molar ratio of 0.6:1:2.7, the suitable reaction condition are the reaction temperature of 160°C and a flow rate of 0.2mL/min . The comparison experiment shows that the QDs synthesized by MF method have better optical and colloidal stability than BT method. Meanwhile, it is also found that the introduction of dBSA as a co-stabilizer can improve the PL intensity and stability of NIR $CuInS_2$/ZnS QDs. For the target cell imaging study, the biomolecules HA and FA were induced for specific surface modification of dBSA-$CuInS_2$/ZnS QDs. Cell imaging and cell viability assays of these biomolecule-modified QDs yielded good results for HepG-2 and Panc-1 cells. Since biofunctionalized QDs can be used as optical probes for in vitro bioimaging, our work will certainly open up an avenue for developing a highly integrated MF system that is capable of preparing high-quality, biocompatible, and easily biofunctionalized near-infrared QDs for direct usage in cell and tumor in vitro imaging work.

Conflicts of interest

There are no conflicts to declare.

Acknowledgements

Project Funded by China Postdoctoral Science Foundation (2019M651959), Postdoctoral Research Funding Program of Jiangsu Province (2018K004B).

Authors' contributions

S.H, K-T. Y and H.M. conceived the concept and experiments. K-T. Y, L.L and Y.T designed some parts of experiment. S.H, B.Z and S.Z carried out the experiment and collected data. S.H. wrote the manuscript, and all authors reviewed and commented on the manuscript

Notes and references

1. G. X. Xu, S. W. Zeng, B. T. Zhang, M. T. Swihart, K. T. Yong and P. N. Prasad, Chemical Reviews, 2016, 116, 12234-12327.
2. L. W. Liu, R. Hu, W. C. Law, I. Roy, J. Zhu, L. Ye, S. Y. Hu, X. H. Zhang and K. T. Yong, Analyst, 2013, 138, 6144-6153.
3. B. Zhang, C. Yang, Y. Gao, Y. Wang, C. Bu, S. Hu, L. Liu, H. V. Demir, J. Qu and K.-T. Yong, Nanotheranostics, 2017, 1, 131-140.
4. B. Zhang, Y. Wang, C. Yang, S. Hu, Y. Gao, Y. Zhang, Y. Wang, H. V. Demir, L. Liub and K.-T. Yong, Physical Chemistry Chemical Physics, 2015, 17, 25133-25141.
5. T. W. Phillips, I. G. Lignos, R. M. Maceiczyk, A. J. deMello and J. C. deMello, Lab on a Chip, 2014, 14, 3172-3180.
6. K. S. Krishna, Y. Li, S. Li and C. S. S. R. Kumar, Advanced Drug Delivery Reviews, 2013, 65, 1470-1495.
7. A. M. Nightingale and J. C. deMello, Advanced Materials, 2013, 25, 1813-1821.
8. J. Edel, R. Fortt, J. Mello and A. Mello, in Micro Total Analysis Systems 2002, eds. Y. Baba, S. Shoji and A. Berg, Springer Netherlands, 2002, DOI: 10.1007/978-94-010-0504-3_57, ch. 57, pp. 772-774.
9. M. Hamamoto, Y. Liang and H. Yagyu, Electronics and Communications in Japan, 2019, 102, 48-54.
10. S. E. Lohse, Size and shape control of metal nanoparticles in millifluidic reactors, 2019.
11. M. Herbst, E. Hofmann and S. Foerster, Langmuir, 2019, 35, 11702-11709.
12. C. D. Ahrberg, J. Wook Choi and B. Geun Chung, Scientific reports, 2020, 10, 1737-1737.
13. S. Hu, S. Zeng, B. Zhang, C. Yang, P. Song, T. J. H. Danny, G. Lin, Y. Wang, T. Anderson, P. Coquet, L. Liu, X. Zhang and K.-T. Yong, Analyst, 2014, 139, 4681-4690.
14. A. M. Nightingale and J. C. de Mello, Journal of Materials Chemistry, 2010, 20, 8454-8463.

View Article Online
DOI: 10.1039/D0LC00202J

15. Y. J. Song, J. Hormes and C. Kumar, Small, 2008, 4, 698-711.
16. A. M. Nightingale, T. W. Phillips, J. H. Bannock and J. C. de Mello, Nature Communications, 2014, 5, 3777.
17. I. Lignos, V. Morad, Y. Shynkarenko, C. Bernasconi, R. M. Maceiczyk, L. Protesescu, F. Bertolotti, S. Kumar, S. T. Ochsenbein, N. Masciocchi, A. Guagliardi, C.-J. Shih, M. I. Bodnarchuk, A. J. deMello and M. V. Kovalenko, Acs Nano, 2018, 12, 5504-5517.
18. T.-L. Cheung, L. Hong, N. Rao, C. Yang, L. Wang, W. J. Lai, P. H. J. Chong, W.-C. Law and K.-T. Yong, Nanoscale, 2016, 8, 6609-6622.
19. G.-X. Liang, M.-M. Gu, J.-R. Zhang and J.-J. Zhu, Nanotechnology, 2009, 20.
20. L. Ye, K. T. Yong, L. W. Liu, I. Roy, R. Hu, J. Zhu, H. X. Cai, W. C. Law, J. W. Liu, K. Wang, J. Liu, Y. Q. Liu, Y. Z. Hu, X. H. Zhang, M. T. Swihart and P. N. Prasad, Nature Nanotechnology, 2012, 7, 453-458.
21. X. W. He, L. Gao and N. Ma, Scientific Reports, 2013, 3, 11.
22. P. M. Valencia, O. C. Farokhzad, R. Karnik and R. Langer, Nature Nanotechnology, 2012, 7, 623-629.
23. D.-H. Tsai, F. W. DelRio, A. M. Keene, K. M. Tyner, R. I. MacCuspie, T. J. Cho, M. R. Zachariah and V. A. Hackley, Langmuir, 2011, 27, 2464-2477.
24. H. Li, Y. Guo, L. Xiao and B. Chen, Analyst, 2014, 139, 285-289.
25. Q. Wang, Y. Kuo, Y. Wang, G. Shin, C. Ruengruglikit and Q. Huang, Journal of Physical Chemistry B, 2006, 110, 16860-16866.
26. J.-H. Wang, H.-Q. Wang, H.-L. Zhang, X.-Q. Li, X.-F. Hua, Y.-C. Cao, Z.-L. Huang and Y.-D. Zhao, Analytical and Bioanalytical Chemistry, 2007, 388, 969-974.
27. X. Luo, P. Su, W. Zhang and C. L. Raston, Advanced Materials Technologies, 2019, DOI: 10.1002/admt.201900488.
28. K. S. Kim, W. Hur, S.-J. Park, S. W. Hong, J. E. Choi, E. J. Goh, S. K. Yoon and S. K. Hahn, Acs Nano, 2010, 4, 3005-3014.
29. S. Hu, Y. Ren, Y. Wang, J. Li, J. Qu, L. Liu, H. Ma and Y. Tang, Beilstein Journal of Nanotechnology, 2019, 10, 22-31.
30. F. Yin, B. Zhang, S. Zeng, G. Lin, J. Tian, C. Yang, K. Wang, G. Xu and K.-T. Yong, Journal of Materials Chemistry B, 2015, 3, 6081-6093.
31. E. Song, W. Han, C. Li, D. Cheng, L. Li, L. Liu, G. Zhu, Y. Song and W. Tan, Acs Applied Materials & Interfaces, 2014, 6, 11882-11890.
32. J. Kim, K. S. Kim, G. Jiang, H. Kang, S. Kim, B.-S. Kim, M. H. Park and S. K. Hahn, Biopolymers, 2008, 89, 1144-1153.